Planar Growth of Pentacene on the Dielectric TiO_2(110) Surface

Valeria Lanzilotto,[†] Carlos Sanchez-Sanchez,[‡] Gregor Bavdek,[¶] Dean Cvetko,[§] Maria F. Lopez,[‡] José A. Martin-Gago,[‡] and Luca Floreano*[,†]

[†]Instituto de Ciencia de Materiales de Madrid (CSIC), C/Sor Juana Ines de la Cruz 3, E-28049 Madrid, Spain

[‡]CNR-IOM, Laboratorio TASC, Basovizza SS-14, Km 163.5, I-34149 Trieste, Italy

[¶]Faculty of Education and [§]Department of Physics, University of Ljubljana, Ljubljana, Slovenia

ABSTRACT: We have studied the growth of pentacene molecules on the unreconstructed and stoichiometric surface of TiO_2(110). At variance with its characteristic homeotropic growth mode, pentacene is found to be physisorbed on this dielectric substrate with its long molecular axis oriented parallel to the surface and aligned along the [001] direction. Pentacene molecules couple side-by-side into long stripes running along the $[1\bar{1}0]$ direction, where the overlayer preserves the substrate lattice periodicity (~6.5 Å). In the opposite direction, head-to-head pentacene repulsion drives the ordering of the stripes, whose spacing simply depends on the surface coverage. By near-edge X-ray absorption, NEXAFS, we have determined the pentacene molecules to be tilted by ~25° off the surface around their long axis. At the monolayer coverage, the pentacene orientation and spacing are very close to that of the (010) bulk planes (also called $a-c$ planes) of pentacene crystals. We have observed that at least two additional layers can be grown on top of the monolayer following a planar configuration. Both the strong side-by-side intermolecular attraction and the full development of the bulklike electronic states, as probed by NEXAFS, suggest an optimal charge transport along the monolayer stripes of lying-down molecules.

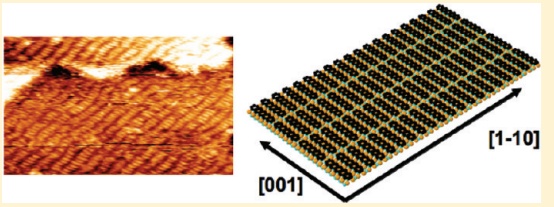

INTRODUCTION

Most of the organic molecules for electronic applications are based on π-conjugated electronic systems, which display a strong tendency to maximize the overlap of the π-orbitals with the electronic cloud of metallic surfaces (i.e., they adsorb flat on metals). On the contrary, they display little interaction with most of the oxide dielectrics, thus favoring the van der Waals intermolecular interaction that drives the molecular assembling. As a consequence, molecular reorientation is typically observed at the interface with electrodes in hybrid devices, thus yielding bad contact resistance because of the formation of topological defects.[1] For a better tailoring of the molecular orientation, alternative routes must be followed such as increasing the device complexity by chemical modification of the electrodes[2] and dielectrics[3] or searching the best matching molecular conformation and substrate structure.

The availability of suitable molecule/substrate pairs is also relevant for the development of specific organic devices (thin film transistors, OTFTs, light emitting devices, OLEDs, and photovoltaic cells, OPVs), where different functionalities are favored by different coupling geometries between the organic molecule and the substrate. For example, planar molecules oriented parallel to the surface of electrodes are favored in the design of bottom-contact OTFTs since the corresponding π-stacking of the molecules in the channel favors the optimal electron transport.[4] On the contrary, light emission is rather enhanced when π-conjugated systems are oriented parallel to the dielectric substrates.

Pentacene is one of the most widely employed molecules for organic devices since it has been used to build OTFTs with high carrier mobility[5,6] and high efficiency OPVs.[7−9] These performances are mainly due to the intrinsic properties of the individual molecules, while the pentacene assembling structure and morphology are much harder to be tailored. In fact, the growth of the molecular crystal proceeds along the (001) natural direction of growth by stacking of layers, where the molecules are packed in a herringbone structure with an orientation almost normal to the stacking layers.[10] The possibility to stabilize a few layers of pentacene in a lying-down geometry would be highly desirable in order to enhance specific functionalities, such as substrate charge transfer and light emission. The formation of a well-ordered first layer where pentacene lays flat has been reported for most of the metal surfaces,[11] but the molecules have a strong tendency to tilt up from the early stage of the second-layer formation.[12,13] Thin films of flat-oriented molecules on metals have been seldom reported, i.e., only when the substrate periodicity closely matches that of the pentacene bulk planes.[14−16] So far, no lying-down layers of pentacene have been reported on dielectric substrates.

TiO_2 is instinctively associated with the engineering of dye-sensitized solar cells, but its high dielectric constant makes it a valuable material also for the fabrication of low threshold voltage and high output current OTFTs.[3] In particular, the rutile TiO_2-(110) surface attracts much attention thanks to the possibility of changing its catalytic and charge transport properties by trimming the concentration of oxygen vacancies in the surface region (either by thermal annealing or by ion bombardment). In fact,

the desorption of oxygen atoms leads to the appearance of a new electronic state in the band gap,[17] which is associated with a redistribution of the local excess of charge among multiple sites around the Ti atoms.[18] This electronic effect on the surface Ti atoms is further enhanced upon the formation of a (1×2) surface reconstruction, induced by high-temperature annealing.[19]

Very recently, the strong structural anisotropy of the TiO_2-(110) surface has been tentatively exploited as a template to drive the oriented growth of planar organic molecules, such as phthalocyanines,[20−22] porphyrins,[23] and perylene derivatives.[24−26] When these molecules adsorb flat onto the substrate, the intralayer lateral transport is inhibited, but a much faster charge transfer to the substrate has been reported.[27] However, this effect is strongly quenched beyond the first monolayer because of the poor coupling, hence ordering, of the next-layer molecules. Structural improvements of the molecular overlayer have been found for the deposition on different TiO_2 faces and reconstructions.[20,22,24]

Apart from the highly symmetric C60 molecule (forming at least one commensurate monolayer[28,29]), the choice of planar molecules better matching the substrate lattice might allow improvement of the coherence of the growing film. This route has been attempted by deposition of uniaxial molecules like anthracene,[30] α-sexithiophene, 6T,[31] and *para*-sexiphenyl, 6P.[32] While a large density of substrate surface defects inhibited the possible ordering of anthracene,[30] the substrate anisotropy was effectively found to drive the azimuthal orientation of 6T and 6P.[33] However, the natural direction of growth of the bulk molecular crystal was still found to dominate the molecular aggregation from the very first layer, that is, standing-up orientation for sexiphenyl and lying-down orientation for sexithiophene (because this orientation is characteristic of the 6T bulk polymorphs[34] and thin films[35]).

Here we show the formation of a compact monolayer of lying-down pentacene on the unreconstructed and stoichiometric TiO_2(110) surface. This ordered phase is formed by molecules oriented along the [001] direction and coupled side-by-side into stripes running in the $[1\bar{1}0]$ direction. The molecules within the stripes have the same spacing of the substrate periodicity, 6.49 Å, and display a tilt of 25° around the long axis. The monolayer phase mimics the structural arrangement of the molecular bulk crystal in the (010), i.e., $a-c$, plane,[10] thus allowing to preserve the lying-down orientation in the next few layers.

EXPERIMENTAL SECTION

We have used several samples of TiO_2(110) from Mateck, with thickness ranging from 0.5 to 1 mm. Samples are attached to a molybdenum spacer by silver paste and slowly heated up to 400° overnight before insertion into the UHV experimental chambers. The sample is mounted on a compact holder (POD) provided with two thermocouples in direct contact with the Mo spacer, a coldfinger for sample cooling, and a filament for sample heating by electron bombardment. The sample temperature is cross-checked by means of the POD K-thermocouples and a pyrometer. The POD is fully interchangeable between the He atom scattering (HAS) apparatus and the ALOISA experimental chamber, which allows us to reproduce the same temperature treatments in the two chambers.

Once outgassed, the surface is prepared by 10−20 min of Ar^+ ion bombardment at 1 keV followed by annealing up to 800°, with a maximum pressure in the 10^{-8} mbar range. After this treatment the sample assumes a characteristic black color with a reflective surface. We have quantitatively verified that this procedure yields the best (1×1) HAS diffraction pattern in terms of both peak intensity and peak width, i.e., lowest density of surface defects and largest domain size (mean terrace width of ∼1000 Å). In these conditions, most of the oxygen vacancies are confined in the subsurface region. This is also confirmed by the almost complete disappearance of the oxygen vacancy band gap state, which may only be detected at resonance with the Ti 2p ionization threshold.[18] Lower temperature annealing (blue sample) yields a larger density of surface defects that also deteriorates the ordering of the pentacene planar phases. Within the Aloisa chamber, a RHEED system is eventually employed to check a posteriori the surface symmetry of both the clean and pentacene-covered substrate. In fact, RHEED illumination produces oxygen vacancies and must be carefully operated.

Pentacene (Sigma, 99.5% purity) is evaporated from home-made crucibles (both tantalum baskets and boron nitride crucibles) operated at 190−200°. The evaporation rate in the HAS chamber is monitored in real time by He scattering, whereas a quartz microbalance is employed in the Aloisa chamber for rate calibration. In the STM apparatus, the evaporation rate is calibrated a posteriori from the molecular density of the planar phases in the first layer. In the latter case, we estimate a coverage uncertainty of 10%. The films are prepared at typical rates in the range of 0.1−1 Å/min.

The HAS apparatus is attached to the branch line of the ALOISA Synchrotron beamline for real time measurements of X-ray photoemission and He scattering. The He diffraction setup, which is described in detail elsewhere,[36] is equipped with a six-degrees-of-freedom manipulator, which allows a precision of 0.005° on its three rotations. The apparatus has a fixed 110° source-to-detector scattering geometry, where one-dimensional diffraction patterns are taken by rotating the manipulator around an axis perpendicular to the scattering plane. The He beam is operated while cooling at liquid nitrogen the nozzle source, which yields a beam wave vector of 6.074 $Å^{-1}$. At the corresponding He beam energy of ∼19 meV, the He atoms cannot perturb the surface atoms/molecules and are scattered at about 3 Å above the nuclei plane, thus probing only the outermost surface charge density (see Figure 4 of ref 37 for a comparison among the probing depth of different surface diffraction techniques). The HAS apparatus allows us to collect consecutive diffraction scans during pentacene deposition, thus monitoring in real time the evolution of the diffraction pattern.

We have employed a linearly polarized photon beam at the ALOISA beamline of the Synchrotron Elettra (Trieste) to measure the near-edge X-ray absorption fine structure, NEXAFS, at the carbon *K*-shell ionization threshold (with ∼90 meV photon energy resolution). NEXAFS spectra are taken by rotating the sample around the photon beam axis (polar scan) while keeping the grazing angle fixed at 6°. A sketch of the scattering geometry can be seen in Figure 1 of ref 37. The NEXAFS signal is collected in partial electron yield by means of a full aperture detector (channeltron) in front of the sample with an electrostatic high-pass filter set to −230 V, in order to reject secondary electrons. The photon energy is calibrated with a precision of 0.01 eV thanks to the carbon absorption feature in the I0 reference (drain) current. The latter has been formerly calibrated by simultaneous acquisition of the C1s $\rightarrow \pi^*$ gas phase transition of CO with the Aloisa in-line windowless ionization chamber.[38]

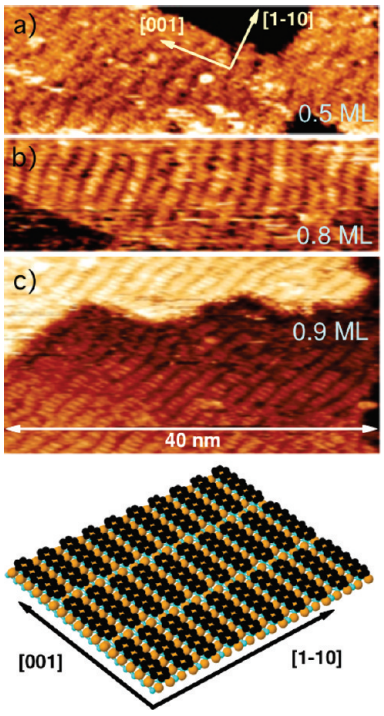

Figure 1. Three STM images taken in constant-current mode with positive sample bias values ranging from 1.0 to 1.8 V and typical tunnel current of 0.15 nA. The images are set to the same horizontal scale of 40 nm. (a) STM image taken at a coverage of ~0.5 ML. The stripes are very irregular and mobile, but, in the image areas where more regular arrangements are seen, one can resolve their inner structure as made of adjacent bright segments, perfectly parallel to the oxygen rows in the [001] direction. (b) At a coverage of ~0.8 ML pentacene, the stripes display a regular spacing, even if their orientation is still not homogeneous. Individual molecules can be clearly resolved within the stripes. Molecules in adjacent stripes are always aligned head-to-head, while side-by-side spacing preserves the substrate periodicity along the $[1\bar{1}0]$ direction. (c) At ~0.9 ML of pentacene, the spacing between the stripes decreases and the stripes run almost homogeneously along the $[1\bar{1}0]$ direction. Bottom: a drawing of the pentacene arrangement at the monolayer coverage. The pentacene register with the substrate is arbitrary and must only be considered as a guide to the eye for the comparison of the molecular orientation and size with the substrate lattice ones.

All STM measurements are carried out at the ESISNA group of the Instituto de Ciencia de Materiales de Madrid (ICMM-CSIC). The UHV chamber is equipped with a commercial room temperature STM (Omicron) driven by a Nanotec electronics, LEED optics, and a cylindrical mirror electron analyzer for Auger spectroscopy. We have used chemically etched tungsten tips prepared in situ by high-temperature annealing and field emission.[39] We have recorded topographical images in the constant current mode using always a positive voltage applied to the sample (empty states) due to the well-known complexity of this substrate for using negative bias.[40] We have analyzed the STM images with the WSxM software from Nanotec.[41]

RESULTS AND DISCUSSION

Monolayer. The (1×1)-$TiO_2(110)$ surface exhibits characteristic oxygen rows protruding over the surface, extending along the [001] direction (lattice unit $a_1 = 2.959$ Å) and spaced by $a_2 = 6.495$ Å in the $[1\bar{1}0]$ direction.[42] In standard STM images

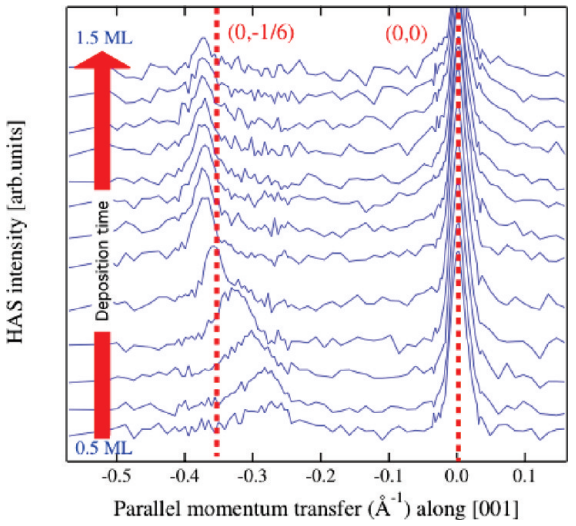

Figure 2. Consecutive HAS diffraction scans taken along the [001] direction during pentacene deposition with the substrate at RT. The scans are vertically displaced by a linear offset, according to the increasing coverage. The bottom scan is taken at a nominal coverage of 0.45 ML and the topmost one at 1.5 ML. Each angular scan is recorded in about 1.5 min, corresponding to the deposition of about 0.08 ML. On the right, a vertical dotted line marks the position of the (0, 0) reflection; an additional vertical dotted line is traced on the left, marking the nominal position of a fractional peak with sixfold periodicity.

(W tip, positive sample bias), this pronounced anisotropy appears as bright lines stemming from the Ti atoms in between the oxygen rows.[40] This large substrate corrugation along the $[1\bar{1}0]$ direction is well suited to accommodate an uniaxial molecule such as pentacene (~5−6 Å wide and ~15.5 Å long) with its long edge aligned parallel to the oxygen rows, as effectively observed. Pentacene molecules result to be very mobile on this substrate already at room temperature, RT, as indirectly confirmed by the difficulty of imaging the surface by scanning tunneling microscopy, STM, in the very low coverage range.

In Figure 1, STM images are shown in the submonolayer range, where the monolayer, ML, is defined as the maximum coverage of pentacene accommodated in the first layer. At a coverage of about 0.5 ML, molecular domains are formed, which are characterized by irregular stripes running in the $[1\bar{1}0]$ direction and roughly spaced by ~20 Å. Notwithstanding the pronounced blurring due to the motion of molecules at this coverage, each stripe can be resolved into small parallel segments that are perfectly aligned along the [001] direction (as determined from STM images where the pentacene stripes coexist with bare TiO_2 areas). Since the length of the segments is in the range of 16 Å, we associate them with lying-down pentacene molecules aligned side-by-side within the stripes, as shown in the drawing of Figure 1. Pentacene growth thus proceeds by an interplay between the molecule-to-substrate interaction (that drives the molecular azimuthal orientation and planar configuration) and the intermolecular side-by-side attraction (that drives the formation of continuous stripes).

At higher coverage, we have observed the emergence of a certain degree of lateral long-range order associated with a straightening of the stripes and a decrease of the interstripe spacing. At 0.8 ML, the stripe spacing is more regular and the stripe shape appears steady, thus confirming the establishment of

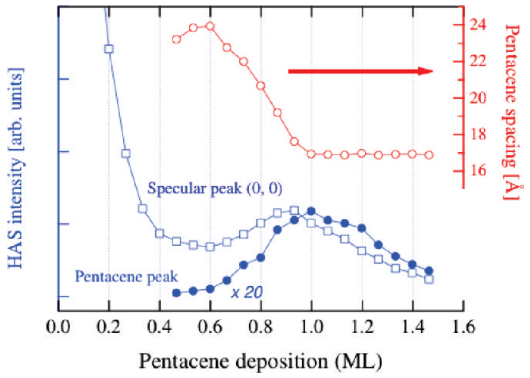

Figure 3. Intensity of the HAS (0, 0) specular reflectivity (open squares) shown together with that of the new diffraction feature (filled circles, amplified by a factor of 20). The variation with coverage of the spacing along the [001] direction, corresponding to the angular position of the new peak, is shown in the upper part of the graphic (open circles, right vertical axis). Data points have been determined from the deposition sequence of the former Figure 2.

an equilibrium phase. As can be appreciated in the middle panel of Figure 1, the molecules of adjacent stripes display a perfect head-to-head alignment along the [001] direction. Additional pentacene deposition decreases further the spacing between the stripes, which also become more regularly aligned along the $[1\bar{1}0]$ direction. Pentacene molecules within the stripes always display the same side-by-side spacing along the $[1\bar{1}0]$ direction that corresponds to the substrate spacing between oxygen rows (see drawing in Figure 1).

In order to have a more quantitative evaluation of the evolution of the stripe spacing, i.e., molecular density, of the growing layer, we have taken consecutive one-dimensional HAS diffraction scans during pentacene deposition. In agreement with the STM sequence, no additional periodicity can be detected along the $[1\bar{1}0]$ direction, whereas new diffraction features appear along the [001] direction from a coverage of 0.5 ML.

A representative set of diffraction scans along the [001] direction is shown in Figure 2, as recorded in a coverage range from 0.5 to 1.5 ML during deposition at 300 K (RT). Initially, the intensity of the specularly reflected (0, 0) peak decreases steeply without broadening, thus indicating the gradual covering of the substrate by uncorrelated molecules. Close to the specular peak, a new incommensurate diffraction feature is formed at about 0.5 ML, which grows in intensity and gradually shifts away from the (0, 0) reflection up to a steady angular position. Further deposition simply decreases the overall intensity of the diffraction pattern. Only when the angular position of the new diffraction peak corresponds to the (0, 1/6) fractional peak do we have observed the emergence of weak second-order peaks of the same sixfold periodicity (both by HAS and RHEED); at different deposition stages, the new diffraction feature only displays a single diffraction order aside the substrate Bragg peaks (0, 0), (0, ±1).

A quantitative analysis of the evolution of the diffraction pattern is shown in Figure 3. The spacing associated with the new diffraction peak is found to match well the spacing between the stripes for the corresponding coverage, as derived from STM images. The (0, 0) reflectivity displays only one weak intensity oscillation with coverage. The appearance of a reflectivity maximum during heteroepitaxial growth is associated with the formation of a new spatially ordered surface (layer). The new diffraction feature appears in correspondence of the shallow minimum of the (0, 0) reflectivity, and its intensity displays a maximum corresponding to the maximum of the (0, 0) reflectivity. The mean spacing associated with the new peak is shown in the upper graphic, where the steady value of 16.9 Å is reached at the intensity maximum of the new peak. As a consequence, we consider this coverage to define the monolayer, i.e., the coverage corresponding to the most dense first layer.

The continuous variation of the stripe spacing from 24 to 16.9 Å, i.e., beyond the commensurate sixfold periodicity (17.7 Å), suggests that the straightening and alignment of the stripes is driven by pentacene head-to-head repulsion without a significative contribution from the substrate atomic structure. Only when the stripe spacing is commensurate with the substrate do we observe the appearance of a few very weak fractional peaks of higher sixfold order. At different coverage, the head-to-head repulsion alone is not strong enough to establish a long-range order and the new diffraction feature simply represents the occurrence of a preferred (most probable) spacing among the stripes, rather than a true periodicity. On the contrary, the substrate corrugation due to the oxygen rows is dictating the pentacene azimuthal orientation and, coupled with the side-by-side pentacene attraction, drives the strictly commensurate side-by-side spacing between the pentacene molecules within the stripes.

Finally, both the absence of an additional periodicity along the $[1\bar{1}0]$ direction and the stripe spacing being only compatible with a single lying-down pentacene molecule suggest that pentacene molecules are all equivalent in the first wetting layer. The monolayer phase yields a molecular density of 0.91 ± 0.01 molecule nm^{-2}. This value is larger than the density of the monolayer phase on Cu(110) (0.83 molecule nm^{-2}), which is already known to allow the growth of a few additional lying-down layers.[16] In particular, the pentacene spacing along the stripes in the substrate $[1\bar{1}0]$ direction perfectly matches the $d_{[100]}$ periodicity (a axis) of the pentacene crystal in the thin film phase, whereas the monolayer head-to-head spacing is ∼8% larger than the $d_{[001]}$ pentacene crystal periodicity (a = 6.49 Å, b = 7.41 Å, c = 14.75 Å).[10] We remark that the molecules in the $a-c$ bulk plane also display a slight rotation around the long axis by ∼25° off the $a-c$ plane because of the pentacene herringbone packing.

Both STM and HAS measurements are concurrent in indicating the lying-down adsorption geometry; however, they do not yield any information about the possible rotation of the molecular plane around its long axis. X-ray absorption spectroscopy is a suitable technique for determining the geometric orientation of the adsorbed molecules. In fact, pentacene is a planar molecule ($D2h$ symmetry), whose transition dipole moment from the s-symmetry core levels to the π^*-symmetry unoccupied molecular orbitals, LUMOs, is oriented perpendicular to the molecular plane. On the contrary, the transition dipole moments to σ^*-symmetry LUMOs are lying within the molecular plane. The intensity of the LUMO resonances at the carbon K-edge thus depends on the orientation of the molecule with respect to the electric field of the photon beam. The occurrence of a preferential orientation of pentacene on $TiO_2(110)$ would allow us to determine its tilting angle by measuring the NEXAFS dichroism of the LUMO resonances at the C K-edge for different orientations of the surface with respect to the linear polarization of the X-ray beam.

The carbon K-edge NEXAFS spectra taken on a monolayer phase for representative surface orientations are shown in

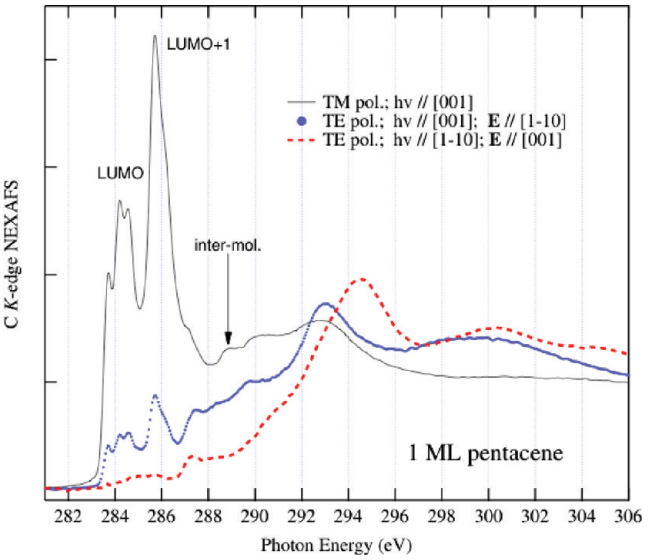

Figure 4. NEXAFS taken at the C *K*-edge in the monolayer phase for two opposite orientations of the surface with respect to the X-ray polarization (TM and TE polarization, full line and markers, respectively), and for two different azimuthal orientations in TE polarization (**E** ∥ [1$\bar{1}$0] and **E** ∥ [001], markers and dashed line, respectively).

Figure 4. In our grazing scattering geometry, the spectra are taken keeping the photon beam at a constant grazing incidence of 6°, while rotating the surface around the beam axis to change its polar orientation θ with respect to electric field, from transverse magnetic (TM, θ = 90°, or *p*-polarization), when the magnetic field is perpendicular to the scattering plane, to transverse electric (TE, θ = 0°, or *s*-polarization). By comparing the spectra taken with the photon beam along the substrate [001] direction, i.e., along the molecular long axis, one notices the strong intensity decrease of the spectral features in the 283−287 eV range, when passing from TM to TE polarization. In fact, this multiplet structure stems from the π-symmetry pentacene LUMO and LUMO+1,[43] and this dichroism indicates that the molecules are adsorbed with a small tilt angle with respect to the surface. An opposite dichroism is also observed for the broad spectral lines in the 292−305 eV range that stem from σ-symmetry LUMOs, indeed.

By fitting the NEXAFS spectra, a quantitative evaluation of the molecular tilting angle γ can be obtained from the LUMO intensity dependence on the polarization angle θ.[44] For a π-plane transition symmetry and twofold surface symmetry, the ratio between the two opposite polarizations I_{TE}/I_{TM} is proportional to $\tan^2\gamma$; thus, we obtain a molecular tilt angle $\gamma = 25° \pm 2°$. This angle is associated with a rotation of pentacene around its long axis, as quantitatively confirmed from the comparison of the NEXAFS spectra taken in TE polarization for different azimuthal orientations of the surface (also see Figure 1 in ref 13 for a sketch of the scattering geometry), where an additional dichroism is detected. As it can be seen in Figure 4, the residual intensity of the π-symmetry LUMOs observed when the beam is oriented along the [001] direction (corresponding to the electric field oriented along the [1$\bar{1}$0] direction) practically vanishes when the surface azimuth is rotated by 90°, bringing the photon beam along the [1$\bar{1}$0] direction. In this case, the absence of π-symmetry resonances implies that the molecular plane is perfectly parallel to the electric field, when the latter is oriented along the [001] direction.

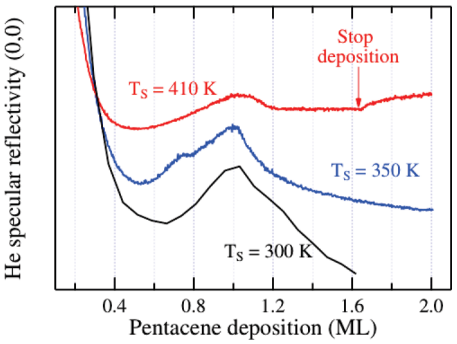

Figure 5. Intensity of the HAS specular reflectivity (0, 0) during deposition at different substrate temperature. See text for details about the deposition curve at 410 K.

We have previously found the same strong azimuthal dichroism for the pentacene nanorails grown on the Au(110) surface, where 1/3 of the molecules lay on its long edge rotated by 90° with respect to the surface.[13] From comparison with the latter system, the tilted molecules are expected to display a strong rotational vibration around the main pentacene axis, which is consistent with the strong Debye−Waller intensity attenuation observed by HAS. We remark that a molecular tilt angle of ∼28° was also reported for anthracene on TiO_2, but for an otherwise disordered monolayer phase, as witnessed by the absence of azimuthal changes, suggesting a mix of lying-down and standing-up molecules.[30] On the contrary, here we can unequivocally state that the pentacene long axis is parallel to the surface.

Finally, the NEXAFS spectrum taken in TM polarization shows additional spectral features at 288.8 and 290 eV, as is typically observed only in thick pentacene films. The identification of these peaks has been controversial in the past since they are typically absent or largely shifted in the single-layer phases.[45,46] In any case, they are expected to yield a negligible contribution to the NEXAFS spectra when the electric field is parallel to the long axis of pentacene, as confirmed by the perfect azimuthal dichroism we observe in TE polarization. From comparison with data and calculations for the case of benzene, there is now a general consensus in assigning the peak at 288.8 eV to the σ^*-state of the C−H bond, while the state at 290 eV has possibly a π^*-character with relevant contributions from Rydberg states.[47] Beyond substrate-induced rehybridization effects, it must be considered that the energy position of the σ^*_{C-H} state is also affected by the stretching of the C−H bond length. In addition, no spectral features can be detected in the gas phase spectra of pentacene at 289−290 eV.[43] Thus, the full development of these NEXAFS resonances can be regarded as the resultant of the intermolecular interaction in the pentacene herringbone packing, i.e., of the interaction of the pentacene rim atoms and bonds with the electronic cloud of adjacent molecules. As a matter of fact, the full bulklike development of these electronic states may be detected at the monolayer thickness only for a homeotropic (standing-up) orientation,[48,49] but, so far, it has never been reported for a lying-down phase, where molecule-to-substrate interactions typically dominate over intermolecular interaction. On the contrary, the present weak interaction with the substrate together with the strong side-by-side attraction and molecular tilting yield an interaction between adjacent pentacene molecules that is strong enough to fully develop a bulklike electronic structure along the stripes, although in a lying-down monolayer phase.

Multilayer. The peculiar pentacene spacing of the monolayer phase, the 25° tilt angle of the molecules, and the occurrence of the fully developed bulklike electronic states are promising conditions for the accommodation of a few additional layers of lying-down molecules. We have first monitored by HAS reflectivity the growth of additional pentacene layers. As it can be seen in Figure 5, at room temperature the (0, 0) reflectivity rapidly vanishes beyond the maximum corresponding to the completion of the first layer. This behavior is indicative of a proliferation of uncorrelated defects (either static or dynamical, like enhanced molecular vibration). At a substrate temperature of 350 K, we have found an improvement of the structural quality of the monolayer (from the peak intensity and width, as measured after cooling the sample to RT), but further deposition simply leads to a gradual vanishing of the monolayer diffraction pattern without the appearance of any additional periodicity. In addition, the corresponding dichroism of the NEXAFS spectra (not shown) indicates that multilayers grown at 350 K display the onset of standing-up molecular clusters already at a nominal thickness of 3 ML. Finally, the monolayer phase is found to correspond to the saturation coverage at T_s = 410 K. In fact, after a small intensity decrease beyond the monolayer maximum, the reflectivity soon reaches a steady intensity. By stopping of the deposition at constant substrate temperature, the (0, 0) intensity quickly recovers the intensity of the monolayer maximum. As a consequence, no second-layer molecules can be accommodated at 410 K on the lying-down pentacene phase, in full agreement with previous findings for the pentacene flat phases on the Au(110) surface.[50]

Notwithstanding the absence of a well-defined diffraction pattern associated with second-layer pentacene, STM images show that pentacene molecules preserve a lying-down geometry at least up to the third layer. In Figure 6, we show second-layer domains measured at a nominal coverage of 1.7 ML, where the molecular packing preserves the striped morphology and intermolecular spacing. The residual molecular vacancy islands, observed in the second layer, are always one-dimensional, and they extend along the stripes; moreover, the stripes adjacent to the pentacene vacancies appear unperturbed. These observations are indicative of a relatively strong intermolecular attraction both side-by-side and with the molecules underneath. This attractive interaction exceeds the head-to-head repulsion that drives the stripe spacing.

Images taken at 2.5 ML in Figure 6 show that third-layer molecules start to lose the striped morphology and grow by squared irregular patches, even if the molecules preserve a certain degree of vertical coherence with the monolayer phase. The early occurrence of the overlayer fragmentation is not surprising, since it was also observed for the more "flexible" system of sexithiophene on Au(110). In the latter case, despite the formation of a perfectly commensurate second layer, the natural herringbone structure (planar orientation in the (120) 6T crystal plane) is recovered at 4 ML, as driven by the strain release (mainly rotational) among adjacent bulk lattice cells.[35] Here the same mechanism is possibly operative both along the pentacene stripes and along the molecular axis. In fact, even if the lateral coupling of the molecules mimics well the herringbone structure along the substrate $[1\bar{1}0]$ direction, one must recall that in the bulk crystal the molecules stacked along the pentacene c axis are tilted with respect to the $a-b$ plane.[10] Thus, apart from the 8% spacing mismatch, the perfect head-to-head azimuthal orientation along the substrate [001] direction is not compatible with the

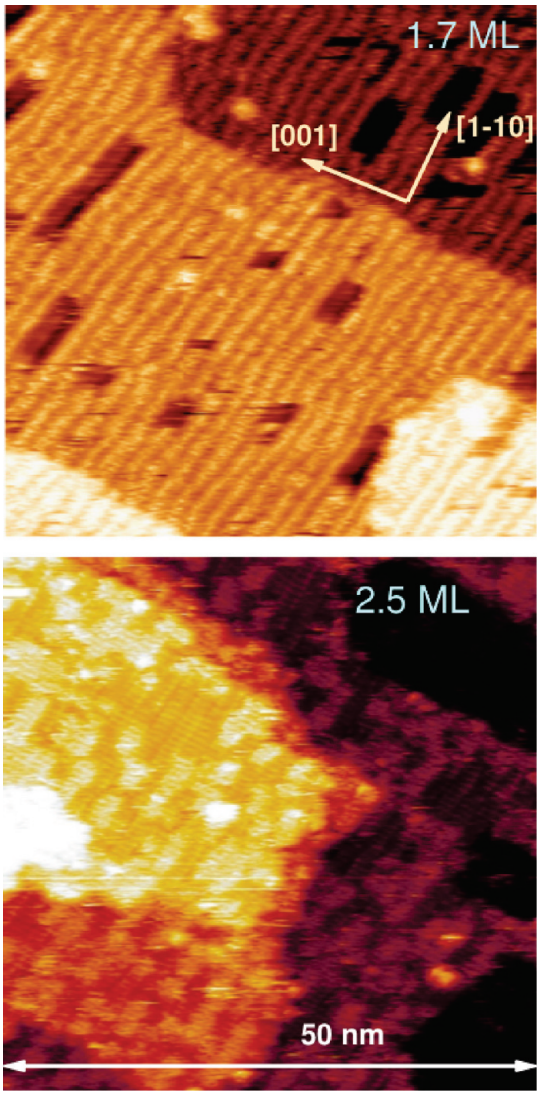

Figure 6. STM images recorded at constant current with a sample bias of 1.8 V. The images are set to the same horizontal scale of 50 nm. Top: at ~1.7 ML, second-layer molecules preserve the striped morphology and the stripes are well aligned along the $[1\bar{1}0]$ direction. Molecular vacancy islands can be appreciated in this compact striped phase. Bottom: at ~2.5 ML, squared irregular islands are formed on top of the striped phase. Resolving individual molecules becomes increasingly difficult in third- and fourth-layer terraces. However, the height of the terrace steps indicates that pentacene preserves its lying-down orientation.

pentacene bulk packing along the c axis, and some azimuthal reorientation of the molecules must take place as soon as the herringbone stacking developes.

The optimal lying-down geometry of these few layer films is confirmed by the polarization dichroism of the NEXAFS spectra. At 3 ML, the NEXAFS spectra of Figure 7 preserve the same dichroic behavior of the monolayer phase. The overall tilt angle increases to 30° that is still compatible with the herringbone bulk packing, also considering a layer-by-layer vertical gradient of the tilt,. Even if we still observe a strong azimuthal dichroism in TE polarization, the NEXAFS spectra display a residual π^*-LUMO intensity when the electric field is oriented along the [001] direction in TE polarization. From comparison with STM images, we attribute this intensity to lying-down molecules that

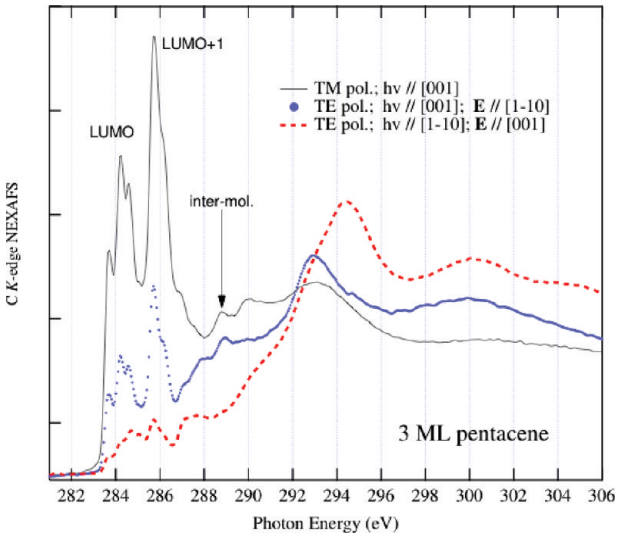

Figure 7. NEXAFS spectra taken at the C *K*-edge for a ~ 3 ML film obtained in two steps by first growing the monolayer at 350 K and evaporating further pentacene at lower substrate temperature. Same polarization conditions of Figure 4.

have slightly changed their azimuthal orientation, rather than to uncorrelated clusters of standing-up molecules.

Due to the high pentacene mobility, we could not follow with sufficient resolution the vertical stacking of the molecules. In particular, by the overall small tilt angle we cannot exclude a close cofacial stacking of the second-layer molecules, a packing structure that has been recently claimed to enhance the pentacene photosensitivity to the solar spectrum.[51] In any case, thanks to the strong molecular coupling along the stripes in the $[1\bar{1}0]$ direction, as also witnessed by the full development of the bulklike electronic states from the first layer, the pentacene stripes may favor the charge mobility parallel to the substrate, although in a lying-down molecular orientation. This is in contrast with what is commonly observed for pentacene[2,5] and most of the oligomers,[4,52] where the intralayer lateral transport is rather enhanced by the homeotropic alignment to the dielectric substrate. The present geometry also implies that the charge transfer at electrodes would be favored in a top-contact architecture. This geometry overcomes the bad contact resistance of the most common bottom-contact geometry, which requires the chemical modification of the electrode surface by a self-assembled monolayer in order to limit the formation of topological defects at the metal/organic interface.[2] In addition, the crystalline nature of the substrate preserves a good structural coherence of the organic semiconductor film without the need of chemical modification of the gate dielectric surface.[3]

CONCLUSION

We have shown that the unreconstructed (1×1)-$TiO_2(110)$ rutile surface is well suited to host the growth of a few planar pentacene layers. The adsorption geometry is dictated by the 6.5 Å periodicity of the substrate that perfectly matches the intermolecular spacing along the *a* axis of the pentacene crystals in the thin film phase. The molecule-to-substrate interaction drives the azimuthal orientation of pentacene along the $[001]$ direction, whereas the intermolecular side-by-side attraction results in the appearance of continuous stripes along the $[1\bar{1}0]$ direction. The molecules within the stripes are tilted around their long axis by 25°. The interstripe spacing decreases with increasing coverage as a result of head-to-head intermolecular repulsion up to the saturation of the first monolayer. The latter displays the full development of the pentacene bulklike electronic states, as probed by NEXAFS resonances. Both the tilting angle and the spacing of the monolayer mimic the structure of the pentacene *a*−*c* crystal planes, thus allowing further deposition of molecules in a lying-down configuration at least up to the third layer. Notwithstanding the overall planar orientation, the strong intermolecular coupling along the stripes suggests an optimal charge mobility parallel to the substrate already from the first layer. At the same time, this geometry implies that a top-contact device architecture would be best suited to limit the formation of defects at the metal/organic interface, i.e., to yield the best performance in terms of charge transfer at the electrodes.

AUTHOR INFORMATION

Corresponding Author

*E-mail floreano@tasc.infm.it.

ACKNOWLEDGMENT

L.F. is grateful to Michele Alagia for fruitful discussions. Financial support from the Spanish CYCIT (MAT2008-1497) and the Ministry of Science and Innovation (CSD2007-41 NANOSELECT) is greatly acknowledged. C.S.-S. is grateful to Ministerio de Educació n for the AP2005-0433 FPU grant. Funding from the European Community Seventh Framework Programme (FP7/2007-2013) under grant agreement no. 226716 is acknowledged.

REFERENCES

(1) Muck, T.; Fritz, J.; Wagner, V. Better bottom contact properties in organic field-effect transistors with ultrathin layers. *Appl. Phys. Lett.* **2005**, *86*, 232101.

(2) Kymissis, I.; Dimitrakopoulos, C. D.; Purushothaman, S. High-performance bottom electrode organic thin-film transistors. *IEEE Trans. Electron Devices* **2001**, *48*, 1060.

(3) Majewski, L. A.; Schroeder, R.; Grell, M. Low-voltage, high-performance organic field-effect transistors with an ultra-thin TiO_2 layer as gate insulator. *Adv. Funct. Mater.* **2005**, *15*, 1017.

(4) Sirringhaus, H.; Brown, P. J.; Friend, R. H.; Nielsen, M. M.; Bechgaard, K.; Langeveld-Voss, B. M. W.; Spiering, A. J. H.; Janssen, R. A. J.; Meijer, E. W.; Herwig, P.; de Leeuw, D. M. Two-dimensional charge transport in self-organized, high-mobility conjugated polymers. *Nature* **1999**, *401*, 685.

(5) Dimitrakopoulos, C. D.; Malenfant, P. R. L. Organic thin film transistors for large area electronics. *Adv. Mater.* **2002**, *14*, 99.

(6) Kitamura, M.; Arakawa, Y. Pentacene-based organic field-effect transistors. *J. Phys.: Condens. Matter* **2008**, *20*, 184011.

(7) Yoo, S.; Domercq, B.; Kippelen, B. Efficient thin-film organic solar cells based on pentacene/C60 heterojunctions. *Appl. Phys. Lett.* **2004**, *85*, 5427.

(8) Mayer, A. C.; Lloyd, M. T.; Herman, D. J.; Kasen, T. G.; Malliaras, G. G. Postfabrication annealing of pentacene-based photovoltaic cells. *Appl. Phys. Lett.* **2004**, *85*, 6272.

(9) Pandey, A. K.; Dabos-Seignon, S.; Nunzi, J.-M. Pentacene: PTCDI-C13H27 molecular blends efficiently harvest light for solar cell applications. *Appl. Phys. Lett.* **2006**, *89*, 113506.

(10) Mattheus, C. C.; Dros, A. B.; Baas, J.; Meetsma, A.; de Boer, J. L.; Palstra, T. T. M. Polymorphism in pentacene. *Acta Crystallogr., Sect. C: Cryst. Struct. Commun.* **2001**, *57*, 939.

(11) Ruiz, R.; Choudary, D.; Nickel, B.; Toccoli, T.; Chang, K.-C.; Mayer, A. C.; Clancy, P.; Blakely, J. M.; Headrick, R. L.; Iannotta, S.; Malliaras, G. G. Pentacene thin film growth. *Chem. Mater.* **2004**, *16*, 4497.

(12) France, C. B.; Schroeder, P. G.; Parkinson, B. A. Direct observation of a widely spaced periodic row structure at the pentacene/Au(111) interface using scanning tunneling microscopy. *Nano Lett.* **2002**, *2*, 693.

(13) Bavdek, G.; Cossaro, A.; Cvetko, D.; Africh, C.; Blasetti, C.; Esch, F.; Morgante, A.; Floreano, L. Pentacene nanorails on Au(110). *Langmuir* **2008**, *24*, 767.

(14) Kang, J. H.; Zhu, X.-Y. Layer-by-layer growth of incommensurate, polycrystalline, lying-down pentacene thin films on Au(111). *Chem. Mater.* **2006**, *18*, 1318.

(15) Casalis, L.; Danisman, M. F.; Nickel, B.; Bracco, G.; Toccoli, T.; Iannotta, S.; Scoles, G. Hyperthermal molecular beam deposition of highly ordered organic thin films. *Phys. Rev. Lett.* **2003**, *90*, 206101.

(16) Söhnchen, S.; Lukas, S.; Witte, G. Epitaxial growth of pentacene films on Cu(110). *J. Chem. Phys.* **2004**, *121*, 525.

(17) Yim, C. M.; Pang, C. L.; Thornton, G. Oxygen vacancy origin of the surface band-gap state of TiO_2(110). *Phys. Rev. Lett.* **2010**, *104*, 036806.

(18) Krüger, P.; Bourgeois, S.; Domenichini, B.; Magnan, H.; Chandesris, D.; Le Févre, P.; Flank, A. M.; Jupille, J.; Floreano, L.; Cossaro, A.; Verdini, A.; Morgante, A. Defect states at the TiO_2(110) surface probed by resonant photoelectron diffraction. *Phys. Rev. Lett.* **2008**, *100*, 055501.

(19) Blanco, M.; Abad, J.; Rogero, C.; Mendez, J.; Lopez, M. F.; Martin-Gago, J. A.; de Andres, P. L. Structure of rutile TiO_2(110)-1 × 2: Formation of Ti_2O_3 quasi-1D metallic chains. *Phys. Rev. Lett.* **2006**, *96*, 55502.

(20) Wang, Y.; Ye, Y.; Wu, K. Adsorption and assembly of copper phthalocyanine on cross-linked TiO_2(110)-(1 × 2) and TiO_2(210). *J. Phys. Chem. B* **2006**, *110*, 17960.

(21) Palmgren, P.; Nilson, K.; Yu, S.; Hennies, F.; Angot, T.; Nlebedim, C. I.; Layet, J.-M.; Le Lay, G.; Göthelid, M. Strong interactions in dye-sensitized interfaces. *J. Phys. Chem. C* **2008**, *112*, 5972.

(22) Godlewski, S.; Tekiel, A.; Prauzner-Bechcicki, J. S.; Budzioch, J.; Szymonski, M. Controlled reorientation of CuPc molecules in ordered structures assembled on the TiO_2(011)-(2 × 1) surface. *Chem. Phys. Chem.* **2010**, *11*, 1863.

(23) Rienzo, A.; Mayor, L. C.; Magnano, G.; Satterley, C. J.; Ataman, E.; Schnadt, J.; Schulte, K.; O'Shea, J. N. X-ray absorption and photoemission spectroscopy of zinc protoporphyrin adsorbed on rutile TiO_2-(110) prepared by in situ electrospray deposition. *J. Chem. Phys.* **2010**, *132*, 084703.

(24) Tekiel, A.; Godlewski, S.; Budzioch, J.; Szymonski, M. Nanofabrication of PTCDA molecular chains on rutile TiO_2(011)-(2 × 1) surfaces. *Nanotechnology* **2008**, *19*, 495304.

(25) Schuster, B.-E.; Casu, M. B.; Biswas, I.; Hinderhofer, A.; Gerlach, A.; Schreiber, F.; Chasseé, T. Role of the substrate in electronic structure, molecular orientation, and morphology of organic thin films: Diindenoperylene on rutile TiO_2(110). *Phys. Chem. Chem. Phys.* **2009**, *11*, 9000.

(26) Simonsen, J. B.; Handke, B.; Li, Z.; Møller, P. J. A study of the interaction between perylene and the TiO_2(110)-(1 × 1) surface-based on XPS, UPS and NEXAFS measurements. *Surf. Sci.* **2009**, *603*, 1270.

(27) Ino, D.; Watanabe, K.; Takagi, N.; Matsumoto, Y. Electron transfer dynamics from organic adsorbate to a semiconductor surface: Zinc phthalocyanine on TiO_2(110). *J. Phys. Chem. B* **2005**, *109*, 18018.

(28) Loske, F.; Bechstein, R.; Schütte, J.; Ostendorf, F.; Reichling, M.; Kühnle, A. Growth of ordered C60 islands on TiO_2(110). *Nanotechnology* **2009**, *20*, 065606.

(29) Fukui, K.-i.; Sakai, M. Formation of one-dimensional C60 rows on TiO_2(110)-1 × 2-cross-link structure and their local polymerization. *J. Phys. Chem. B* **2006**, *110*, 21118.

(30) Reiss, S.; Krumm, H.; Niklewski, A.; Staemmler, V.; Wöll, Ch. The adsorption of acenes on rutile TiO_2(110): A multi-technique investigation. *J. Chem. Phys.* **2002**, *116*, 7704.

(31) Ivanco, J.; Haber, T.; Krenn, J. R.; Netzer, F. P.; Resel, R.; Ramsey, M. G. Sexithiophene films on ordered and disordered TiO_2-(110) surfaces: Electronic, structural and morphological properties. *Surf. Sci.* **2007**, *601*, 178.

(32) Resel, R.; Oehzelt, M.; Lengyel, O.; Haber, T.; Schülli, T. U.; Thierry, A.; Hlawacek, G.; Teichert, C.; Berkebile, S.; Koller, G.; Ramsey, M. G. The epitaxial sexiphenyl (001) monolayer on TiO_2-(110): A grazing incidence X-ray diffraction study. *Surf. Sci.* **2006**, *600*, 4645.

(33) Koller, G.; Berkebile, S.; Ivanco, J.; Netzer, F. P.; Ramsey, M. G. Device relevant organic films and interfaces: A surface science approach. *Surf. Sci.* **2007**, *601*, 5683.

(34) Servet, B.; Ries, S.; Trotel, M.; Alnot, P.; Horowitz, G.; Garnier, F. X-ray determination of the crystal structure and orientation of vacuum evaporated sexithiophene films. *Adv. Mater.* **1993**, *5*, 461.

(35) Prato, S.; Floreano, L.; Cvetko, D.; De Renzi, V.; Morgante, A.; Modesti, S.; Biscarini, F.; Zamboni, R.; Taliani, C. Anisotropic ordered planar growth of α-sexithienyl thin films. *J. Phys. Chem. B* **1999**, *103*, 7788.

(36) Cvetko, D.; Lausi, A.; Morgante, A.; Tommasini, F.; Prince, K. C.; Sastry, M. Compact He beam scattering apparatus for surface studies. *Meas. Sci. Technol.* **1992**, *3*, 997.

(37) Floreano, L.; Cossaro, A.; Gotter, R.; Verdini, A.; Bavdek, G.; Evangelista, F.; Ruocco, A.; Morgante, A.; Cvetko, D. Periodic arrays of Cu-phthalocyanine chains on Au(110). *J. Phys. Chem. C* **2008**, *112*, 10794.

(38) Floreano, L.; Naletto, G.; Cvetko, D. R, G.; Malvezzi, M.; Marassi, L.; Morgante, A.; Santaniello, A.; Verdini, A.; Tommasini, F.; Tondello, G. Performance of the grating-crystal monochromator of the ALOISA beamline at the ELETTRA synchrotron. *Rev. Sci. Instrum.* **1999**, *70*, 3855.

(39) Mendez, J.; Gomez-Herrero, J.; Pascual, J.; Baro, A. M. Formation of new terraces via diffusion induced by the field gradient in scanning tunneling microscopy. *Appl. Phys. A: Mater. Sci. Process.* **1998**, *66*, S767.

(40) Sanchez-Sanchez, C.; Gonzalez, C.; Jelinek, P.; Mendez, J.; de Andres, P. L.; Martin-Gago, J. A.; Lopez, M. F. Understanding atomic-resolved TiO_2(110)-(1 × 1) STM images by DFT calculations. *Nanotechnology* **2010**, *21*, 405702.

(41) Horcas, I.; Fernandez, R.; Gomez-Rodriguez, J. M.; Colchero, J.; Gomez-Herrero, J.; Baro, A. M. WSXM: A software for scanning probe microscopy and a tool for nanotechnology. *Rev. Sci. Instrum.* **2007**, *78*, 013705.

(42) Busayaporn, W.; Torrelles, X.; Wander, A.; Tomic, S.; Ernst, A.; Montanari, B.; Harrison, N. M.; Bikondoa, O.; Joumard, I.; Zegenhagen, J.; Cabailh, G.; Thornton, G.; Lindsay, R. Geometric structure of TiO_2(110)(1 × 1): Confirming experimental conclusions. *Phys. Rev. B* **2010**, *81*, 153404.

(43) Alagia, M.; Baldacchini, C.; Betti, M. G.; Bussolotti, F.; Carravetta, V.; Ekström, U.; Mariani, C.; Stranges, S. Core-shell photoabsorption and photoelectron spectra of gas-phase pentacene: Experiment and theory. *J. Chem. Phys.* **2005**, *122*, 124305.

(44) Stöhr, J. *NEXAFS Spectroscopy*; Springer-Verlag: Berlin, Germany, 1992; paragraph 9.4.2.

(45) Söenchen, S.; Lukas, S.; Witte, G. Epitaxial growth of pentacene films on Cu(110). *J. Chem. Phys.* **2004**, *121*, 525.

(46) Käfer, D.; Witte, G. Evolution of pentacene films on Ag(111): Growth beyond the first monolayer. *Chem. Phys. Lett.* **2007**, *442*, 376.

(47) Kolczewski, C.; Puttner, R.; Martins, M.; Schlachter, A. S.; Snell, G.; SantÕAnna, M. M.; Hermann, K.; Kaindl, G. Spectroscopic analysis of small organic molecules: A comprehensive near-edge X-ray-absorption fine-structure study of C6-ring-containing molecules. *J. Chem. Phys.* **2006**, *124*, 034302.

(48) Chiodi, M.; Gavioli, L.; Beccari, M.; Di Castro, V.; Copssaro, A.; Floreano, L.; Morgante, A.; Kanjilal, A.; Mariani, C.; Betti, M. G. Interaction strength and molecular orientation of a single layer of pentacene in organic−metal interface and organic−organic heterostructure. *Phys. Rev. B* **2008**, *77*, 115321.

(49) Jia, Z.; Lee, V. W.; Kymissis, I.; Floreano, L.; Verdini, A.; Cossaro, A.; Morgante, A. in situ study of pentacene interaction with archetypal hybrid contacts: Fluorinated versus alkane thiols on gold. *Phys. Rev. B* **2010**, *82*, 125457.

(50) Floreano, L.; Cossaro, A.; Cvetko, D.; Bavdek, G.; Morgante, A. Phase diagram of pentacene growth on Au(110). *J. Phys. Chem. B* **2006**, *110*, 4908.

(51) Huang, L.; Rocca, D.; Baroni, S.; Gubbins, K. E.; Buongiorno Nardelli, M. Molecular design of photoactive acenes for organic photovoltaics. *J. Chem. Phys.* **2010**, *130*, 194701.

(52) Murphy, A. R.; Fréchet, J. M. J. Organic semiconducting oligomers for use in thin film transistors. *Chem. Rev.* **2007**, *107*, 1066.